第36卷第5期
2017年10月

红外与毫米波学报
J. Infrared Millim. Waves

Vol. 36, No. 5
October, 2017

文章编号：1001－9014(2017)05－0569－06

DOI:10.11972/j.issn.1001－9014.2017.05.010

Characteristics of the spectral lines of immersion gratings

TANG Qian[1,2,3], GUO Li-Xin[1*], ZHAO Bao-Chang[4]

(1. School of Physics and Optoelectronic Engineering, Xidian University, Xi'an 710071, China;
2. State Key Laboratory of Transient Optics and Photonics, Chinese Academy of Sciences, Xi'an 710119, China;
3. Key Laboratory of Optoelectronic Devices and Systems of Ministry of Education and Guangdong Province, Shenzhen University, Shenzhen 518060, China;
4. Xi'an Institute of Optics and Precision Mechanics of Chinese Academy of Sciences, The Space Optical Technology Research Department, Xi'an 710119, China)

Abstract: Immersion gratings are typically used in the infrared spectral band in which optical materials with high refractive index. Some issues inevitably arise due to their special operating mode. And they are critical to the application of immersion gratings. This study investigated the relations between the lengths of the long- and short-wave of normal gratings. For the features of the relevance of the refractive index with wavelength, the short-wave infrared spectral band (1.5～2.5 μm) was taken as an example to analyze the change characteristics of spectral line location and spectral resolution of immersion gratings. Results showed that when immersion gratings were adopted, significant differences were observed in the distribution of spectral lines as compared with normal gratings, and "trapezoidal" spectral lines tilted. For short-wave infrared spectral lines, the inclination of the "trapezoidal" spectral lines became more apparent due to larger changes in the refractive index of the medium. When Littrow conditions were registered with long-wave length (2.5 μm), the spectral line tilted toward the short-wave end. When registration was done with short-wave length (1.5 μm), the spectral line tilted toward the long-wave end, and the Littrow wavelength drifted away from the central wavelength. The refractive index had a few changes at the thermal infrared spectral band. The tilt of "trapezoidal" spectral lines was smaller and more similar to that of normal gratings. The spectral resolution of immersion gratings varied due to changes in the refractive index. At the same order, the wavelength increased, and resolution increased; between various orders, the order decreased, and the resolution decreased. Meanwhile, considering that the high-order resolution was larger than the low-order's, the ratio of the lengths of spectral lines at various orders no longer meet the relation of normal gratings.

Key words: grating, immersion, refractive index, spectral line drift
PACS: 42.25.Fx, 07.57.Ty, 95.75.Fg, 95.55.Cs

浸入式光栅谱线特性

唐　茜[1,2,3], 郭立新[1*], 赵葆常[4]

(1. 西安电子科技大学,物理与光电工程学院,陕西 西安　710071;
2. 中国科学院西安光学精密机械研究所,瞬态光学与光子技术国家重点实验室, 陕西 西安　710119;
3. 深圳大学,光电子器件与系统教育部/广东省重点实验室,广东 深圳　518060;
4. 中国科学院西安光学精密机械研究所,空间光学应用研究室,陕西 西安　710119)

摘要:浸入式光栅常应用于光学材料折射率较高的红外谱段.其特殊的工作模式会产生一系列普通反射式光栅不需面临的问题,而它们对于浸入式光栅的应用却十分重要.论文推导了普通光栅长波端与短波端谱线长度的关系.针对折射率与波长相关的特点,以短波红外(1.5～2.5 μm)为例,分析其谱线位置分布及光谱分辨

Received date: 2017-04-28, **revised date**: 2017-08-28　　**收稿日期**:2017-04-28, **修回日期**:2017-08-28
Foundation items:Supported by (1) the National Natural Science Foundation of China (61501361); (2)State Key Laboratory of Transient Optics and Photonics, Chinese Academy of Sciences (SKLST201509); (3) Key Laboratory of Optoelectronic Devices and Systems of Ministry of Education and Guangdong Province(GD201712); (4)Open Research Fund of Key Laboratory of Spectral Imaging Technology, Chinese Academy of Sciences (LSIT201506) and (5)the Fundamental Research Funds for the Central Universities(JB160509)
Biography:唐　茜(1986-),女,河南新乡人,讲师,博士,主要从事偏振光谱信息获取及处理方面的研究. E-mail: qtang@xidian.edu.cn
* **Corresponding author**:E-mail:lxguo@xidian.edu.cn

率变化特性.结果表明,浸入式光栅谱线分布相较于普通光栅有明显差异,“梯形”谱线会发生倾斜.在折射率变化较大的短波红外谱段,“梯形”谱线倾斜程度较明显.在以长波(2.5 μm)配准 Littrow 条件时,谱线向短波端倾斜,以短波(1.5 μm)配准时向长波端倾斜,且 Littrow 波长均漂离中心波长.由于折射率在热红外谱段变化较小,“梯形”谱线倾斜较小,更接近普通光栅情况.浸入式光栅的光谱分辨率随折射率变化而改变,同级中,波长增大分辨率增大;各级间,级数减小分辨率减小.同时,由于高级次(短波)分辨率大于低级次(长波),因此各级谱线长度之比不再满足普通光栅中的比例关系.

关 键 词:光栅;浸入式;折射率;谱线漂移

中图分类号:TN214,P412 **文献标识码**:A

Introduction

In aerospace applications, especially those tasks for monitoring the Earth's atmospheric composition, the use of instruments with ultrahigh spectral resolution is often necessary to measure the scattering and transmission spectra of the Earth's atmosphere[1-3]. The grating spectrometers, such as SCIAMACHY and TROPOMI, are extensively applied due to its high resolution and wide range of spectral bands[4-5]. The immersion gratings can substantially increase angular dispersion in comparison with normal gratings[6], thus significantly reducing the size of grating and equipment, or significantly increasing spectral resolution under the premise of maintaining the existing volume of grating.

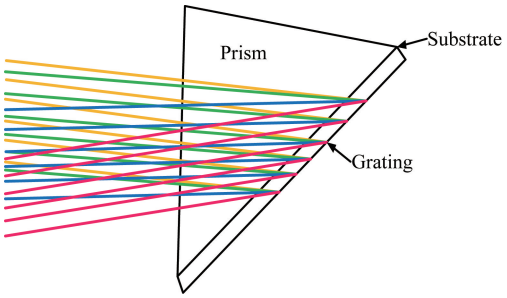

Fig. 1 Structure chart of immersion gratings
图 1 浸入式光栅结构图

The structure chart of immersion gratings is shown in Fig. 1. The main difference between immersion gratings and normal gratings ($n = 1$, n is the refractive index of the medium) is that the refractive indexes of the media. As an example, for common materials of infrared spectral bands, such as silicon and germanium, the refractive indexes of them are 3.4 and 4.1, respectively. If the same spectral resolution is reached, the volume of immersion gratings is only $1/n^3$ of normal gratings. Conversely, the spectral resolution of immersion gratings is n times of normal gratings. The effect of shrinkage in size or improvement in resolution is significant. Thus, the immersion gratings are mainly used in infrared spectral bands.

Numerous countries have invested a considerable amount of manpower, material, and financial resources to study immersion gratings for their distinct advantages[7-8]. Consensus has been reached on the basic principles of immersion gratings, and application researches have been extensively conducted globally[9]. Due to their unique working modes, however, immersion gratings still encounter a range of new problems that must be researched promptly, such as the influence of medium absorption on light intensity distribution[10]. Currently, the characteristics of the spectral lines of immersion gratings have not been encountered in related researches. Such problem is critical to the design and application of immersion grating spectrometers. This research carried out analysis and discussion on this problem.

1 Analysis on the characteristics of spectral line distribution

As no dispersion occurs in the air's refractive index ($n \equiv 1$), symmetrically distributed trapezoids for diffraction spectral lines at various orders are imaged on the CCD focal plane when normal reflection gratings are used (see Fig. 2).

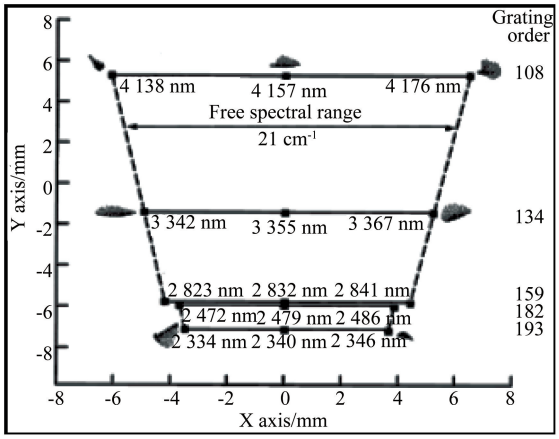

Fig. 2 Spot diagram of the wavelength selected in the working spectral band[11]
图 2 工作谱段中所选波长的点列图[11]

The relations between the lengths of long and short waves of normal gratings working in the air are mathematically derived, as follows.

For the same equipment, the wave number intervals of long-and-short waves are identical, with the working spectral band of $\lambda_{short} \sim \lambda_{long}(\mathrm{nm})$. The wave number interval of the instrument is assumed to be $N(\mathrm{cm}^{-1})$, and the sampling interval of spectra is assumed to be $a(\mathrm{nm})$.

i) Pixel number when λ_{short} is classified

The corresponding wave number of λ_{short} is $\dfrac{10^7}{\lambda_{short}(\mathrm{nm})}$, and the corresponding wave number of λ_{short}

$+\Delta\lambda_{short}$ is $\frac{10^7}{\lambda_{short}(nm)} - N(cm^{-1})$. Therefore,

$$\Delta\lambda_{short} = \frac{\frac{10^7}{\lambda_{short}(nm)} - \lambda_{short}(nm)}{\frac{10^7}{\lambda_{short}(nm)} - N(cm^{-1})} \quad . \quad (1a)$$

The pixel number of λ_{short} is:

$$M_1 = \frac{\Delta\lambda_{short}(nm)}{a} = \left[\frac{\frac{10^7}{\lambda_{short}(nm)} - \lambda_{short}(nm)}{\frac{10^7}{\lambda_{short}(nm)} - N(cm^{-1})}\right] / a \quad . \quad (1b)$$

ii) Pixel number when λ_{long} is classified

The corresponding wave number of λ_{long} is $\frac{10^7}{\lambda_{long}(nm)}$, and the corresponding wave number of λ_{long} $+\Delta\lambda_{long}$ is $\frac{10^7}{\lambda_{long}(nm)} - N(cm^{-1})$. Therefore,

$$\Delta\lambda_{long} = \left|\lambda_{long}(nm) - \frac{10^7}{\frac{10^7}{\lambda_{long}(nm)} - N(cm^{-1})}\right| \quad . \quad (2a)$$

The pixel number of is:

$$M_2 = \frac{\Delta\lambda_{long}(nm)}{a} = \left|\left[\lambda_{long}(nm) - \frac{10^7}{\frac{10^7}{\lambda_{long}(nm)} - N(cm^{-1})}\right] / a\right| \quad . \quad (2b)$$

The lengths ratio of spectral lines of λ_{long} and λ_{short} is the ratio of CCD pixel numbers, each accounting for:

$$M_2 = \frac{\Delta\lambda_{long}/a}{\Delta\lambda_{short}/a} = \frac{\Delta\lambda_{long}}{\Delta\lambda_{short}} = \frac{\lambda_{long}(nm) - \frac{10^7}{\frac{10^7}{\lambda_{long}(nm)} - N(cm^{-1})}}{\frac{\frac{10^7}{\lambda_{short}(nm)} - \lambda_{short}(nm)}{\frac{10^7}{\lambda_{short}(nm)} - N(cm^{-1})}} = \frac{N\lambda^2_{long}(nm)[10^7 - N(cm^{-1}) \cdot \lambda_{long}(nm)]}{N\lambda^2_{short}(nm)[10^7 + N(cm^{-1}) \cdot \lambda_{short}(nm)]} \quad , (3)$$

Considering that $10^7 \gg \lambda_{long}$ (nm), $10^7 \gg \lambda_{short}$ (nm), so

$$\frac{M_2}{M_1} \approx \frac{N\lambda^2_{long}(nm)}{N\lambda^2_{short}(nm)} = \frac{\lambda^2_{long}(nm)}{\lambda^2_{short}(nm)} \quad . \quad (4)$$

Note that the computational analysis in this case is based on derivation under ideal conditions. In practical engineering applications, the relations of spectral line lengths obtained on the CCD focal plane do not strictly comply with the ratio of $\lambda^2_{long}/\lambda^2_{short}$ due to the nonlinearities of grating dispersion and other reasons. This problem will be studied and presented in a subsequent work.

The design of the spectrometer based on the technical index presented in Table 1 is taken as an example to analyze the variation in the distribution of immersion gratings in relation to normal gratings working in the air.

1.1 Distribution of grating spectral lines working in the air

Figure 3 presents the spectral line distribution on CCD when normal gratings are adopted under the spectral band of 1.5 ~ 2.5 μm and working series of the 180th order (1.5 μm) to the 108th order (2.5 μm). Clearly, the diffraction angles for the central wavelengths under all orders are all 63.5°. The diffraction angle at the long-wave end gradually decreases as the order increases (the wavelength decreases). The diffraction angle at the short-wave end gradually increases as the order increases (and the wavelength rises). Theoretically, the ratio of the spectral line length of the long-wave AB (i.e., 2.5 μm, the 108th order) and the spectral line length of the short wave CD (i.e., 1.5 μm, the 180th order) meets the proportional relation derived in Eq. 4.

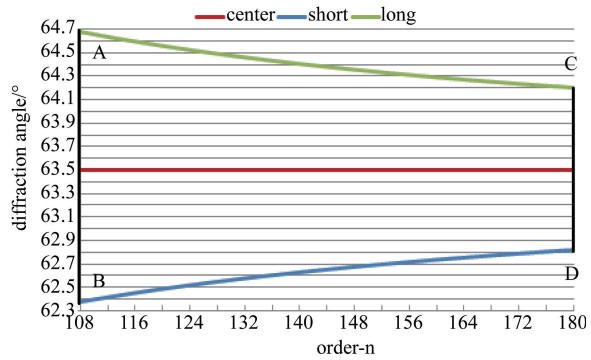

Fig. 3　Distribution of the spectral lines of normal gratings
图 3　普通光栅谱线在 CCD 上的分布

$$\frac{AB}{CD} = \frac{\lambda_{long}{}^2}{\lambda_{short}} = \left[\frac{2.5}{1.8}\right]^2 = 2.77^X \quad . \quad (5)$$

1.2 Spectral line distribution of immersion gratings

When the light is dispersed by immersion gratings, dispersion occurs inside the immersion medium. The Cauchy dispersion formula reveals that the refractive index is a function of the wavelength, where a, b, and c are the values which differ according to the substance examined.

$$n(\lambda) = a + \frac{b}{\lambda^2} + \frac{c}{\lambda^4} \quad . \quad (6)$$

This study takes Si as grating material for which the refractive index distribution curve of 1.5 ~ 2.5 μm spectral bands at normal temperature is shown in Fig. 4.

Table 1　Technical index of Spectrometer
表 1　光谱仪技术参数

project	working spectral band	series	free spectral range	blaze angle of gratings	grating constant	pixel size	spectral resolution	focal length
	μm	order	cm^{-1}	°	mm	mm	nm/2pix	mm
index parameters	1.5 ~ 2.5	180 ~ 108	40	63.5	0.043 903 146	0.05	0.1	90.69

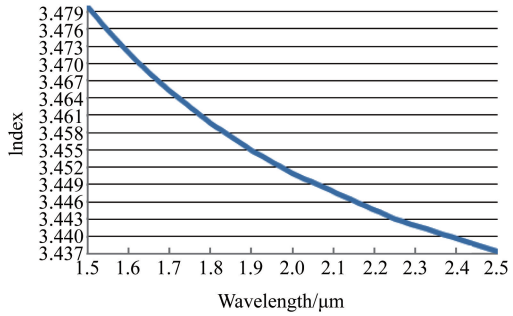

Fig. 4 Refractive index of Si (1.5 ~ 2.5 μm)
图 4 硅的折射率(1.5 ~ 2.5 μm)

The case presented in Fig. 5 differs from that in Fig. 3, as shape of the spectral line on the CCD focal plane twists. When the Littrow condition is registered by the 108th order (2.5 μm), as shown in Fig. 5, the green spot of each order represents the diffraction angle of the short-wave end, the red spot represents the diffraction angle of the central wavelength, and the blue spot represents the diffraction angle of the long-wave end. Lines connecting the spots of different colors indicate the diffraction angle distribution of the short-wave end wavelength, central wavelength, and long-wave end wavelength of each order from the 108th order to the 180th order.

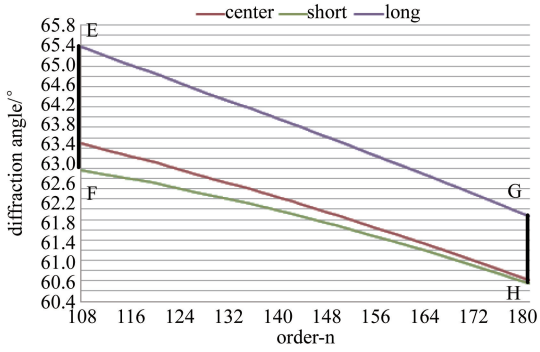

Fig. 5 Spectral line distribution of immersion gratings
图 5 浸入式光栅谱线在 CCD 上的分布

Figure 5 shows the spectral line distribution of immersion gratings. EF is the spectral line length of the long wave (i.e., 2.5 μm, the 108th order) and GH is the spectral line length of the short wave (i.e., 1.5 μm, the 108th order). Moreover, the "trapezoid" of the spectral line tilts.

The following conclusions can be drawn based on the figures presented in this study.

(1) Considering the changes in the refractive index with the wavelength, when Littrow conditions are registered by the 108th order (2.5 μm), the spectral lines of each order gradually drift toward the short-wave end. Similarly, when Littrow conditions are registered by the 180th order (1.5 μm), the spectral lines of each order gradually drift toward the long-wave end.

(2) When the central wavelength of the 108th order meets Littrow conditions, the central wavelength of each order progressively deviates from such conditions. Furthermore, the wavelength that meets Littrow conditions gradually increases. At the 135th order, the wavelength that meets Littrow conditions is the wavelength of the long-wave end. For a higher order, all wavelengths in the spectral bands of such order deviate from Littrow conditions. At this point, the diffraction efficiency is lowered.

(3) The spectral line length of the order for the shortest wavelength (i.e., 1.5μm, the 180th order in this study) increases, and no longer complies with the condition of $[\lambda_{long}/\lambda_{short}]^2$, and turns into EF/GH = 1.7× due to changes in the refractive index. This proportion is associated with the characteristics of the refractive indexes of the selected materials.

(4) Considering the aforementioned condition of spectral line drift, the number of spectral dimensional pixel must increase, and some blank pixels should be reserved when the CCD is selected.

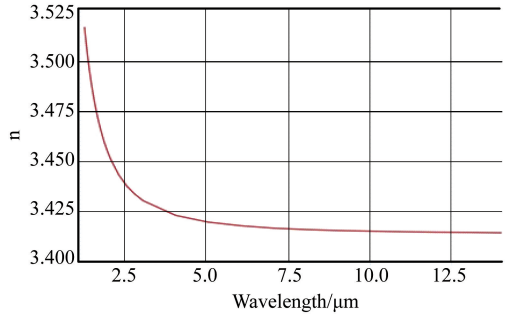

Fig. 6 Refractive index of Si (1.2 ~ 14 μm)[12]
图 6 硅的折射率(1.2 ~ 14 μm)[12]

Figure 6 presents the refractive index curve of Si in infrared spectral bands. In the spectral band of 1.2 ~ 2.5 μm, significant changes are observed in the refractive index. For the spectral band of 2.5 ~ 5 μm, the changes in the refractive index tend to flatten, and only slight changes occur in the refractive index for the spectral band of 7.5 ~ 14 μm. The above analysis indicates that variations in the shape of the spectral line of the detector result from changes in the refractive index. In the region where changes in the refractive index are observed, e.g., in the wave band of 1.5 ~ 2.5 μm, as shown in Fig 5, the "inclination" degree of the spectral line is larger. Therefore, immersion gratings are applied in the thermal infrared spectral band for which minimal variation occurs in the refractive index, such as the spectral band of 8 ~ 14 μm. The "inclination" degree of such spectral line will be significantly improved, similar to the situation of normal gratings.

2 Analysis of the characteristics of immersion grating spectra

Firstly, the 108th order with the central wavelength λ_C of 2.5 μm was taken as an example to calculate the influence of the refractive index on the spectral resolution and analyze the characteristics when the wavelength interval is 0.5 nm (i.e., the detector's CCD interval of 5 pixels).

Table 2 presents the 108th order central wavelength λ_C and $\lambda_C + 0.5$ nm wavelength, as well as their refractive indexes, which are substituted into the grating diffraction formal [20]:

$$m\lambda = d \cdot n \cdot (\sin\theta_C + \sin\theta) \quad , \quad (7)$$

where m represents the order, λ represents the wavelength, d represents the grating constant, n represents the refractive index, θ_C represents the blaze angle of gratings, and θ represents the diffraction angle.

Table 2　108th order central wavelength λ_C, $\lambda_C + \triangle\lambda$, and their refractive indexes

表 2　中文表示 108 级中心波长 λ_C, $\lambda_C + \triangle\lambda$ 及其折射率

wavelength/μm	refractive index
2 500.000	3.439 437 1
2 500.000 +0.5	3.439 427 8

(a) For λ = 2 500.000 nm, n = 3.439 437 1

$108 \times 0.002\ 500\ 0 = 0.043\ 903\ 146 \times 3.439\ 437\ 1 \times (\sin 63.5° + \sin\theta)$

We derive:

$$\begin{cases} \theta = 63.267\ 977\ 746\ 487\ 162° \\ \underline{\Delta\theta} = 0.232\ 022\ 253\ 512\ 838° \\ \overline{\Delta\theta} = 0.798\ 049\ 572\ 662\ 065° \end{cases}$$

where θ is the diffraction angle, $\Delta\theta$ is the angle including of the diffraction angle and the blaze angle in the crystal, and $\overline{\Delta\theta}$ is the angle including of the diffraction angle and the blaze angle outside of the crystal.

(b) For λ = (2 500.000 +0.5) nm, n = 3.439 427 8

$108 \times 0.002\ 500\ 5 = 0.043\ 903\ 146 \times 3.439\ 427\ 8 \times (\sin 63.5° + \sin\theta)$

We derive:

$$\begin{cases} \theta = 63.314\ 184\ 682\ 529\ 941° \\ \underline{\Delta\theta} = 0.185\ 815\ 317\ 470\ 059° \\ \overline{\Delta\theta} = 0.639\ 110\ 495\ 218\ 192° \end{cases}$$

Therefore,

(1) The difference of the diffraction angles of the two beams outside of the crystal (the angular dispersion) can be calculated as: $\Delta\theta' = 0.158\ 939\ 077\ 443\ 873°$;

(2) The interval of the two beams on the focal plane (the linear dispersion):

$l = f \times \tan\Delta\theta = 0.251\ 575\ 631\ 381\ 874$ mm;

However, the theoretical value should be 5×0.05 mm = 0.25 mm. Compared with the theoretical value, the linear dispersion increases by 0.63% and the spectral resolution increases by 0.63%.

Under a wave number interval of 40 cm^{-1}, the 108th order spectral domain is 2 487.5621 nm −2 512.562 3 nm. Table 3 presents the short-wave end wavelength, central wavelength, long-wave end wavelength, and their corresponding refractive indexes.

Table 3　108th order λ_S, λ_C, λ_L, and their refractive indexe

表 3　108 级 λ_S, λ_C, λ_L 及其折射率

wavelength/μm	refractive index/%
2 487.562 1	3.439 671 5
2 500.000	3.439 437 1
2 512.562 3	3.439 204 0

λ_S and λ_L are calculated using the same methods (see Table 4 for results).

Table 4　108th order λ_S, λ_C, λ_L and the changes in their spectral resolutions

表 4　108 级 λ_S, λ_C, λ_L 及其光谱分辨率变化

wavelength/μm	changes in spectral resolution/%
λ_S2 487.562 1	−2.84
λ_C2 500.000 0	+0.63
λ_L2 512.562 3	+5.11

Fig. 7 presents the changes in the spectral resolution with the wavelength in the 108th order spectral domain.

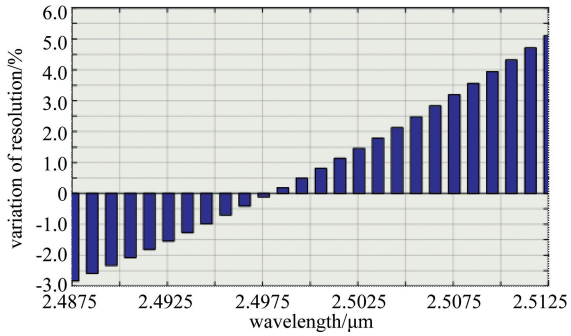

Fig. 7　Trend of changes in the spectral resolution of the spectral band of the 108th order

图 7　108 级谱段光谱分辨率变化趋势

In the spectral band of the 108th order, negative values appear in the region where the wavelength lies. At this point, the spectral resolution is smaller than the theoretical value, i. e., the linear dispersion on CCD is smaller than 0.25 mm. The spectral resolution increases as the wavelength rises. Zero value appears at the position of 2 498 nm. Thereafter, the spectral resolution continues to increase.

Similarly, the trend of the changes in the spectral resolution of the 135th order and the 180th order can be obtained, as shown in Fig. 8.

Analysis of Figs. 7-8 show that at the same order, the spectral resolution increases with the rise in the wavelength, and the trend of changes approximates linearity.

The changes in the spectral resolutions of λ_S, λ_C, and λ_L of various orders are shown in Fig. 9. With an increase in the order (decrease in wavelength), the spectral resolution shows a rising trend, and the three curves exhibit linearity. The trend of changes in the spectral resolution and in the refractive index are similar. That is, the longer the wavelength, the slower the changes in the refractive index. In addition, the increment in the spectral resolution is also decreasing and even displays negative growth.

3　Conclusion

In this research, analysis of the distributional characteristics of immersion grating spectra is conducted. In addition, the derivation of the relation between the lengths of the long- and short-wave ends of normal gratings was explored. Hence, this study suggests the following:

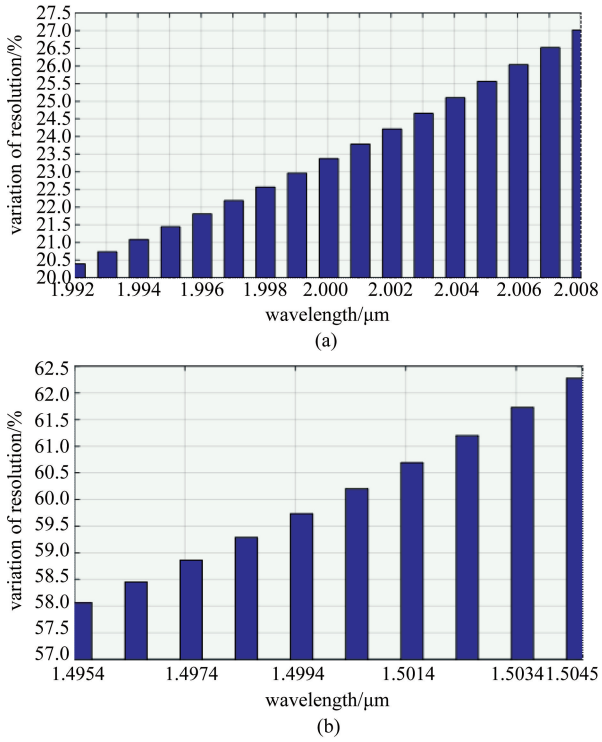

Fig. 8 Trends of changes in the resolution of the spectral bands of the 135th order (a) and the 180th order(b)
图8 135级以及180级谱段分辨率变化趋势(a) 135级谱段分辨率变化趋势,(b) 180级谱段分辨率变化趋势

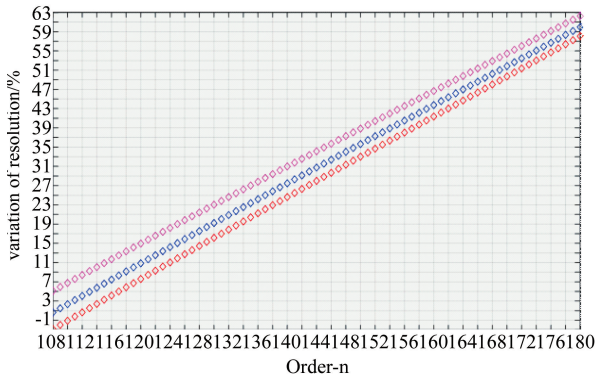

Fig. 9 Changes in the spectral resolutions of λ_S, λ_C, and λ_L of various orders
图9 各级的 λ_S、λ_C 和 λ_L 光谱分辨率变化

(1) The spectral lines of immersion gratings form a tilted trapezoid, whereas the spectral lines of normal reflection gratings appear to be a symmetrical trapezoid under ideal conditions. When Littrow conditions are registered by the 108th order (2.5 μm), the spectral lines of various orders gradually drift toward the short-wave end. When Littrow conditions are registered by the 180th order (1.5 μm), the spectral lines of various orders gradually drift toward the long-wave end. Variations in the shape of spectral lines are caused by the changes in the refractive index with the wavelength. As the spectral lines tilt, "blank reservation" for the edge should be fully considered when the detector is selected.

(2) Under ideal conditions, the spectral lines of normal gratings between various orders meets the relation of $[\lambda_{long}/\lambda_{short}]^2$. However, given that the refractive index of immersion media decreases as the wavelength rises, the ratio of the lengths of the spectral lines between various orders is smaller than $[\lambda_{long}/\lambda_{short}]^2$, while the shape of their spectral lines tilts.

(3) The trends of changes in the spectral resolution and in the refractive index are similar. The longer the wavelength, the slower the change in the refractive index. Meanwhile, the increment in the spectral resolution also decreases, and even displays negative growth. The spectral resolution of immersion gratings varies accordingly as well. At the same order, the wavelength rises, and the spectral resolution increases; between various orders, the order decreases (i. e., the wavelength rises), and the spectral resolution decreases. If Littrow conditions are registered by the 108th order (2.5 μm) in the working spectral band, then the full spectral bands will certainly meet the requirement of spectral resolutions.

The analytical results of this study are significant to the analysis of immersion grating spectra, the design of spectral components, and the selection of optical system detectors. Spectral line drift resulting from other aspects, such as grating constant errors, blaze angle changes and spectral calibration will be analyzed and discussed in a future work.

References

[1] BAI Wen-Guang, ZHANG Peng, ZHANG Wen-Jian, *et al.*, An efficient method for hyper-spectral infrared atmospheric [J]. *J. Infrared Millim. Waves*(白文广, 张鹏,张文建. 一种高效计算高光谱分辨率红外大气辐射传输的方法. **红外与毫米波学报**),2016, **35**(1): 99 - 108.

[2] Mu TK, Zhang CM, Jia CL, *et al.* Static hyperspectral imaging polarimeter for full linear stokes parameters. *Optics Express*, 2012, **20**(16):18194 - 18201.

[3] Zhang CM, Jian XH. Wide-spectrum reconstruction method for a birefringence interference imaging spectrometer. *Optics Letters*, 2010, **35**(3):366 - 368.

[4] Hu H, Hasekamp O, Butz A, *et al.*, The operational methane retrieval algorithm for tropomi [J]. *Atmos. Meas. Tech*, 2016, **9**(11): 5423 - 5440.

[5] Kavitha M, Nair P R., Region-dependent seasonal pattern of methane over indian region as observed by sciamachy [J], *Atmos. Environ*, 2016, **131**: 316 - 523.

[6] Higuchi Y, Ishii Y, Hadama K, *et al.* Polarization insensitive silicon immersion grating based on total internal reflection[J], *Opt. Express*, 2013,**21**(8),9664 - 9673.

[7] Rusu CE, Oguri M, Minowa Y, *et al.* Subaru telescope adaptive optics observations of gravitationally lensed quasars in the sloan digital sky survey [J], *Mon. Not. R. Astron. Soc*, 2016, **458**(1):2 - 55.

[8] Ge J, Zhao B, Powell S, *et al.* An infrared high resolution silicon immersion grating spectrometer for airborne and space missions [C] *Proc. SPIE.* **9143** (2014) 9143:1434T - 1 ~ 10.

[9] Ikeda Y, Kobayashi N, Sarugaku Y, *et al.* Machined immersion grating with theoretically predicted diffraction efficiency[J], *Appl. Opt*, 2015, **54**: 5193.

[10] TANG Qian, QIU Yue-Hong, ZHAO Bao-Chang, *et al.* Research of the immersion grating diffraction pattern[J], *Acta Photonica Sinica* (唐茜,邱跃洪,赵葆常), 2014, **43**(11): 1105002 - 1 ~ 7.

[11] Marsh JP, Mar DJ, Jaffe DT, Production and evaluation of silicon immersion gratings for infrared astronomy[J], *Appl. Opt*, 2007, **46**:3400.

[12] Li HH, Refractive index of silicon and germanium and its wavelength and temperature derivatives[J], *Phys. Chem. Ref. Data*, 1980, **9**:561.